Available online at www.sciencedirect.com
ScienceDirect
Journal of Sound and Vibration 305 (2007) 333–347
JOURNAL OF SOUND AND VIBRATION
www.elsevier.com/locate/jsvi

Short Communication

Time-domain computation of muffler frequency response: Comparison of different numerical schemes

A. Broatch*, J.R. Serrano, F.J. Arnau, D. Moya

CMT - Motores Térmicos, Universidad Politécnica de Valencia, Camino de Vera s/n, 46022-Valencia, Spain

Received 8 November 2005; received in revised form 22 December 2006; accepted 2 April 2007

Abstract

A comparative study of the performance of different schemes used to solve one-dimensional gas flow equations when applied to the computation of the frequency response of exhaust mufflers is presented. Simple but representative systems with well-known acoustic behaviour were considered. Apart from the classical Lax–Wendroff and MacCormack schemes, the total variation diminishing schemes, flux corrected transport techniques or the innovative space–time conservation element and solution element method were considered. The results provide guidelines for a proper choice of the numerical scheme, taking into account the mesh spacing.

1. Introduction

The use of numerical tools for exhaust noise prediction has become a commonplace in industrial practice in the last years [1]. Two main development lines can be distinguished: on one hand, the extension of the capabilities of classical linear acoustic codes initially conceived for muffler performance prediction, so that they may also include a suitable representation of the engine as a noise source; on the other hand, the extension of the capabilities of time-domain one-dimensional unsteady flow simulations originally conceived for engine performance prediction so that they may also include suitable representations for complex realistic mufflers.

In the first case, the main problem comes from the use of linear time-invariant source models to represent an intrinsically nonlinear and time-variant process, as it is the interaction between the cylinders and the exhaust system. This is not a problem when computations in the time domain are used, since both nonlinearity and time-variance are accommodated in a natural fashion. However, the limitations of time-domain models appear mainly in issues related to the description of the silencers and the details of the flow at the open end. As indicated above, these models derive, in general, from calculation programs initially conceived for flow computations from the point of view of performance, to which an emission model has been added to permit the estimation of exhaust noise. It has been shown [2] that usual emission models (monopole or piston) produce a reasonable noise prediction, given that a suitable estimation of the flow fluctuation at the open end

*Corresponding author. Tel.: +34 963 879 650; fax: +34 963 877 659.
E-mail address: abroatch@mot.upv.es (A. Broatch).

0022-460X/$ - see front matter © 2007 Elsevier Ltd. All rights reserved.
doi:10.1016/j.jsv.2007.04.023

is available, in most conditions, with the only exception of low engine speeds, where backflow into the tailpipe may occur and the flow patterns downstream of the open end are likely to become extremely complex. Therefore, it may be stated that the critical point lies in the estimation of the flow fluctuation at the open end which, in short, is obtained from the solution of the one-dimensional unsteady non-homentropic mass, momentum and energy equations. These governing equations, ignoring viscosity, form a non-homogeneous hyperbolic system that can only be solved by means of numerical methods.

The accuracy of the solution obtained depends mainly on two factors: the numerical method chosen to solve the flow equations throughout the ducts of the exhaust system, and the representativity of the boundary conditions used to obtain the flow values at the endpoints of those ducts (most notably, at the open end). The focus of this communication is precisely on the influence of the numerical method. First contributions found in the literature [3] were based on different implementations of the method of characteristics but, being a first-order method, its intrinsically dissipative character produces an undesired high-frequency filtering effect which may be unimportant for performance studies, but clearly affects its suitability for noise prediction [4]. In this sense, recent work is mainly oriented to the use of second-order techniques, which do not exhibit such dissipative behaviour.

Regarding second-order techniques, Onorati et al. [5] compared finite elements methods (FEM) with finite difference schemes, their results indicating the higher accuracy of the FEM, but also the greater computational time required. In fact, the lower computational effort of finite difference schemes makes them suitable even for long duration calculations, such as those involved in engine transient operation modelling [6], and thus the study presented here is focused on such techniques. A summary of the different schemes considered, with pertinent references, is given in Appendix A; now, only their application to noise prediction will be briefly reviewed.

Different predictor–corrector methods have been proposed, such as that described in Ref. [7] or the MacCormack scheme [8–10]. Also, the two-step Lax–Wendroff method has been applied to exhaust noise prediction [8,10,11]. Selamet [12] proposed a finite difference scheme and presented its evaluation in terms of frequency response. Finally, the relatively recent CE–SE method (“conservation element–solution element”) was first applied to exhaust noise studies by Onorati [8]. In all the cases, the results shown suggest that any filtering effects are much less important that those associated with the use of the method of characteristics. In these methods, however, the management of the boundary conditions at the duct endpoints is not straightforward and, in general, it is necessary to consider some approach to the method of characteristics in the vicinity of the boundaries. In this way, the boundary conditions are expressed in terms of the characteristics variables, with which they admit a relatively simple formulation. The precise procedure used in this work was described in detail in Ref. [9] and summarized in Appendix B.

An additional handicap of finite differences schemes is that they exhibit numerical dispersion, this is, wave propagation velocity is a function of frequency, and this in turn produces spurious oscillations in the vicinity of discontinuities in the variables defining the flow, the eventual effect of such oscillations on the frequency spectrum being quite unpredictable. Different techniques have been developed with the purpose of eliminating such unphysical oscillations, most notably the flow corrected transport (FCT) and total variation diminishing (TVD) methods. Direct comparison of methods with respect to numerical dispersion have been widely studied in the field of computational aeroacoustics [13,14], but to the authors’ knowledge, these techniques have not been applied to noise studies in internal combustion engine modelling and thus an assessment of the eventual influence of their use on frequency results is missing. Only in the case of the scheme proposed by Selamet [12] such a study appears to be available [15].

In this paper a comparison between numerical schemes has been performed in order to determine their performance from the point of view of frequency response evaluation. Simple but representative systems of well-known acoustic behaviour (expansion chambers and Herschel-Quincke ducts) were considered. The precise configurations considered are described in Section 2, together with the methodology followed to obtain the corresponding transmission loss. The results obtained are described and discussed in Section 3, with special emphasis on the trade-offs between quality of the results, computational time requirement and the mesh spacing used. Finally, in Section 4 some conclusions are pointed out.

2. Study definition and methodology

In order to check the performance of the different numerical schemes, two simple but representative geometries with well-known acoustic behaviour were chosen: (i) expansion chambers, in which the influence of the muffler volume and the effects associated with transmission and reflection at area discontinuities are present, and (ii) Herschel-Quincke ducts, where phenomena related with wave interference between parallel branches may be studied. Thus, these two geometries, represented in Fig. 1, allow for the study of the main reactive attenuation mechanisms occurring in practical mufflers. The precise geometries used are described in Table 1.

In the case of the expansion chambers, the aim was to guarantee an essentially longitudinal wave propagation, and thus the length to diameter ratios were chosen so that a one-dimensional calculation such as that performed was realistic for a sufficiently wide frequency range. In the case of the Herschel-Quincke ducts, two parameters were modified: the total cross section (i.e. the addition of the cross sections of the two branches) and the lengths of the branches. The total cross section was set to two different values: that corresponding to the cross section of the duct upstream and downstream of the Herschel-Quincke duct (corresponding to a diameter of 50 mm) and to twice that value. With respect to the lengths, the ratio between the lengths of the two branches has been kept constant and equal to 2, and the addition of both lengths has been varied.

The numerical schemes tested were: (i) two centred schemes (two-step Lax–Wendroff and MacCormack predictor–corrector; (ii) four high-resolution schemes: the FCT method (based on the Lax–Wendroff scheme), two TVD schemes (one using Sweby's flux limiting techniques and the other using Harten's correction techniques) and the CE–SE scheme. With this choice a representative set of currently used numerical schemes is available that should provide a rather complete picture of the problem. Information on the details of these schemes can be found, for instance, in Ref. [16], where an evaluation of their behaviour in the time-domain was performed. Here, only a brief description with relevant references is given in Appendix A. In all the cases,

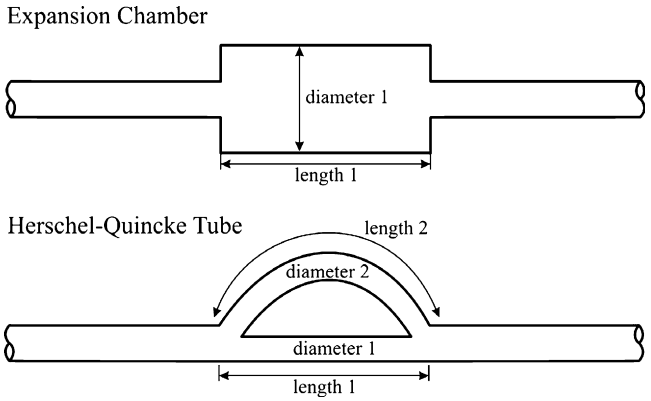

Fig. 1. Schemes of the geometries considered.

Table 1
Summary of geometries considered

Case	Length 1 (mm)	Diameter 1 (mm)	Length 2 (mm)	Diameter 2 (mm)
Chamber 1	450	154	–	–
Chamber 2	300	154	–	–
H-Q 1	450	36	900	36
H-Q 2	225	36	450	36
H-Q 3	450	36	900	62
H-Q 4	225	36	450	62

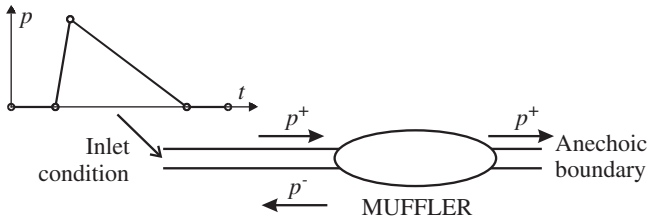

Fig. 2. Sketch of the methodology used for transmission loss computation.

four different mesh spacings (2, 5, 10 and 20 mm) were used in order to analyse the sensitivity of the frequency response obtained from the different methods and allow comparison of their performance.

The transmission loss has been chosen as a suitable magnitude representative of the frequency response of a given muffler. It is defined in terms of a logarithmic ratio between the acoustic power incident on the muffler and the acoustic power transmitted by the muffler. Assuming that the cross section of the ducts upstream and downstream of the muffler are the same, the transmission loss reduces to the ratio between the amplitudes of the incident and the transmitted waves. In order to compute this amplitude ratio, an impulsive excitation has been assumed at the inlet of the upstream duct, and an anechoic termination has been considered at the outlet of the downstream duct, so that a suitable reproduction of the experimental conditions used in the impulse method [17] is achieved. A sketch of the calculation procedure is shown in Fig. 2.

The excitation chosen was as follows: an abrupt pressure rise up to 8.5 kPa (relative) in a very short time interval (0.2 ms), and then a pressure decrease back to ambient pressure after a relatively short time (17 ms). Such an excitation provides an essentially flat spectrum for the wave incident on the muffler, so that relevant results may be obtained at all the frequencies of interest [17]. In addition, the excitation adopted does not include any superimposed mean flow, and thus, only the mean flow related to the pressure pulse has been considered. As it was reported in Ref. [17] the effects of this flow are similar to an equivalent mean flow.

As pointed out in the introduction, boundary conditions are handled by means of the variables associated with the methods of characteristics, this is, the non-dimensional Riemann variables λ and β and the non-dimensional entropy level A_A (the procedure that allows linking these variables at the duct boundaries with the numerical schemes used in the ducts is summarized in Appendix B). Here, the boundary condition used at the upstream duct inlet is given by:

$$\lambda = 2(p/p_0)^{(\gamma-1)/2\gamma} - 1,$$

$$\beta = A_A = 1, \tag{1}$$

where p is the pressure excitation, p_0 is a reference pressure and γ is the specific heat ratio. The second condition forces that the flow at the duct inlet is defined by a simple progressive wave, which is related to the assumed pressure excitation p by the first condition. The boundary condition corresponding to an anechoic termination at the outlet of the downstream duct is simply

$$\beta = A_A. \tag{2}$$

With these considerations, the transmitted amplitude may be obtained directly from the Fourier analysis of the pressure computed downstream of the muffler, whereas the incident amplitude can be obtained assuming that the pressure upstream of the muffler may be written as [18]

$$(p/p_0)^{(\gamma-1)/2\gamma} = (p^+/p_0)^{(\gamma-1)/2\gamma} + (p^-/p_0)^{(\gamma-1)/2\gamma} - 1. \tag{3}$$

Here p^+ and p^- are wave components given by

$$p^+ = p_0\left\{\frac{1}{2}\left(1 + \left[\frac{p}{p_0}\right]^{(\gamma-1)/2\gamma}\left[1 + \frac{\gamma-1}{2}\frac{u}{a}\right]\right)\right\}, \tag{4}$$

$$p^- = p_0\left\{\frac{1}{2}\left(1+\left[\frac{p}{p_0}\right]^{(\gamma-1)/2\gamma}\left[1-\frac{\gamma-1}{2}\frac{u}{a}\right]\right)\right\}, \quad (5)$$

where a is the instantaneous speed of sound and u is the instantaneous particle velocity of the gas. Now, the incident amplitude may be obtained from the Fourier analysis of p^+ as given by Eq. (4).

3. Results and discussion

As commented before, muffler models are evaluated here in the context of a complete engine simulation aiming at exhaust noise prediction. A wave action model (WAM) able to model whole engines has been used but, in this work, only the components of the mufflers studied have been modelled. Computation time is thus a relevant issue, even if computer times for the simulations performed in this work are rather small, and thus it will be now briefly addressed, before passing on to the evaluation of the frequency behaviour.

As an arbitrary time unit, the time required by the WAM with the CE–SE method has been chosen. In Fig. 3 computation times for each method, averaged over all the geometries considered for a given mesh spacing, are shown. Clearly, the Lax–Wendroff method (and the MacCormack method, which is virtually undistinguishable from the former and has not been plotted) is the faster one. High-resolution schemes are slower, as expected, the CE–SE method being the fastest among these, but, even so, taking about double the time than the simple centred schemes. The longest time corresponds to the TVD scheme with Harten flux correction.

The computation times in Fig. 3 are obtained as a result of the complexity of the codes used to solve the flow through the ducts. Fig. 4 shows a comparison of the CPU steps for each method. In this case, only the operations belonging to the method have been considered and the rest of operations (the resolution of the boundary conditions, the heat transfer and the friction calculations, etc.) that are common in all cases have been omitted. The FCT is a particular case, in the sense that the code includes an iterative process. For this reason, the total CPU steps of this scheme are the result of a constant quantity plus a variable quantity depending on the iterations needed to converge. In Fig. 4 only one iteration (in a different grey tone) has been represented. Comparing all the methods, Fig. 4 shows similar trends as Fig. 3 but with bigger differences due to the fact that the common calculations (i.e. boundary conditions, heat transfer, etc.) are not considered.

Of course, the mesh spacing has a paramount influence on computation time. In order to check the sensitivity of the different methods tested to the mesh spacing, in Fig. 5 the same methods as in Fig. 3 are considered, but now plotting the relative influence of this parameter on the computation time for each of the schemes. Since it was checked that computation time scales approximately with the inverse of the square of the mesh spacing, the magnitude chosen was the square root of the ratio of the computation time consumed

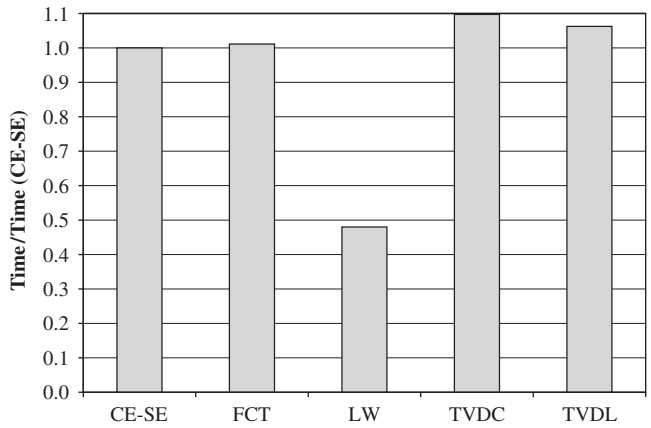

Fig. 3. Comparison of computation time (relative to CE–SE) for different schemes and equal mesh spacing: conservation element–solution element (CE–SE), flow corrected transport (FCT), two-step Lax–Wendroff (LW), total variation diminishing with flux correction (TVDC), total variation diminishing with flux limitation (TVDL).

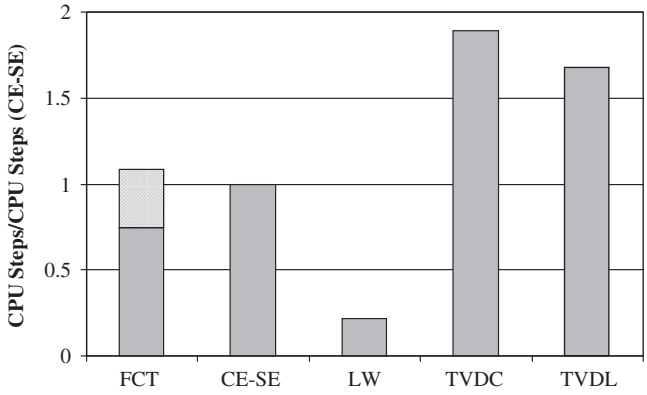

Fig. 4. Comparison of CPU steps for each calculation node.

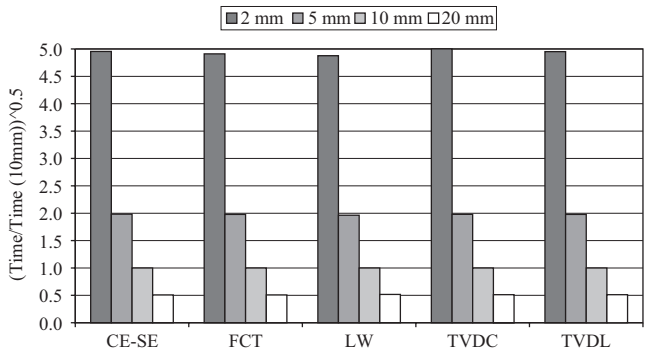

Fig. 5. Comparison of computation time (relative to that obtained with a mesh spacing of 10 mm for each scheme) for the schemes considered with different mesh spacings. Legend as in Fig. 3.

Table 2
Numerical results

Numerical scheme	CPU steps	PPW	Theoretical computational cost
Lax–Wendroff	404	28	11312
CE–SE	1845	37	68265
FCT	1378 + 624	452	904904
TVDC	3494	41	143254
TVDL	3094	42	129948

with a given spacing to that consumed with a reference spacing, which was taken arbitrarily to be 10 mm. It is apparent from Fig. 5 that the relative influence of mesh spacing is substantially the same for all the cases considered, and thus combined analysis of Figs. 3 and 5 permits a precise assessment of the computational cost of a given choice of scheme and mesh spacing.

A more practical result is to compare the computational effort required to achieve a certain accuracy. As an example, the accuracy to reproduce the resonance frequency with the Herschel-Quincke tube H-Q 4 has been compared. Considering a phase error lower than 0.2%, the points per wavelength (PPW) needed to reach that accuracy are obtained from the results with different mesh sizes. Table 2 shows the comparison of the theoretical computational effort for different schemes multiplying the CPU steps times the PPW. As it can be observed in Table 2, the Lax–Wendroff scheme presents the lowest computational effort and CE–SE is the

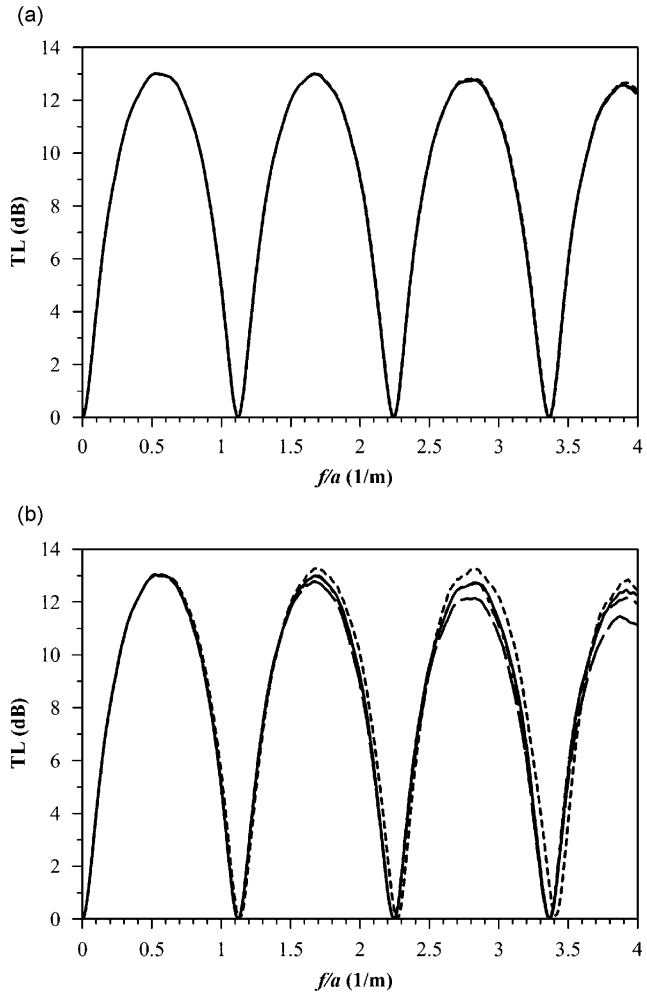

Fig. 6. Comparison of transmission loss computed with different schemes and mesh spacings in chamber 1: (a) mesh of 2 mm, (b) mesh of 20 mm. CE–SE (solid), FCT (dotted), Lax–Wendroff (dash–dot), TVD with flux correction (dash).

best among high-resolution schemes. In addition, it is possible to state that flux corrected techniques are not suitable for acoustic applications.

Focusing now on the influence of the numerical scheme and the mesh spacing on the results obtained for the frequency response, in Fig. 6 the transmission loss of one of the expansion chambers as computed by different numerical methods is shown as a function of the ratio of the frequency f to the speed of sound a. Results depicted in Fig. 6(a) were obtained with a mesh spacing of 2 mm, whereas for those plotted in Fig. 6(b) a mesh spacing of 20 mm was used. It is apparent that for the small mesh spacing all the methods provide substantially the same result; only the FCT method, and only at frequencies above the cut-off frequency of the first transversal mode (which corresponds to $f/a \sim 3.8\,\mathrm{m}^{-1}$ for the geometry considered) presents some very small differences.

However, for the large mesh spacing it is apparent that relatively important differences appear between the different methods. The Lax–Wendroff and the CE–SE methods are not too sensitive to the mesh spacing, producing acceptable results whose quality degrades progressively as frequency increases, but still with small differences with respect to the small mesh spacing. However, both the FCT and the TVD with flux correction (results for the other TVD scheme are very similar and have not been included for clarity) exhibit clear deviations from the results shown in Fig. 6(a). In the case of the TVD scheme, it is apparent that the transmission loss at the attenuation maxima becomes lower as frequency increases; on the contrary, for the

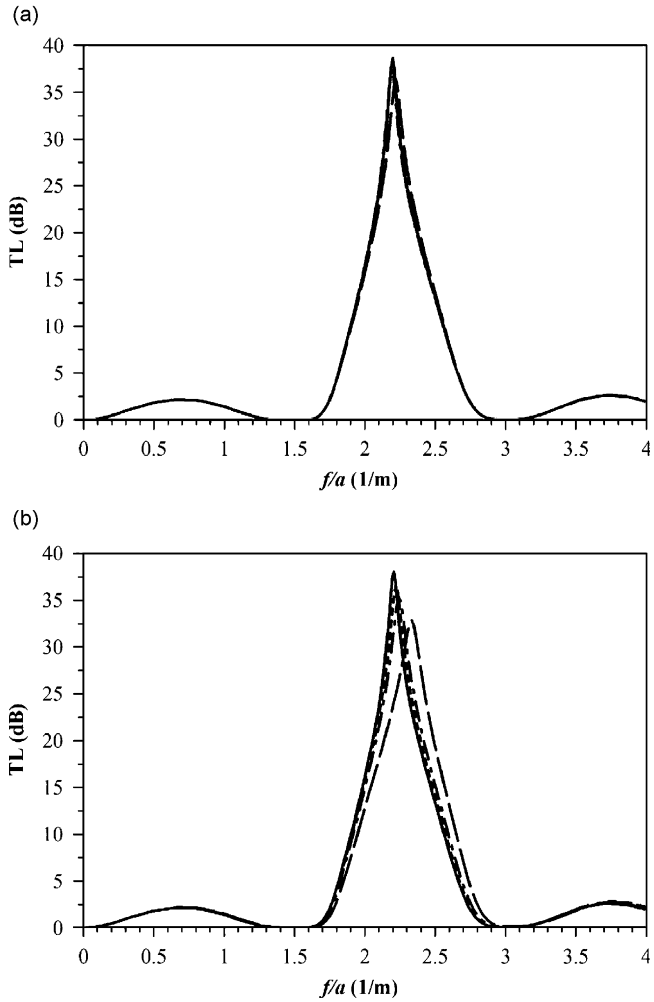

Fig. 7. Comparison of transmission loss computed with different schemes and mesh spacings in H-Q 4: (a) Lax–Wendroff, (b) FCT. Meshes: 2 mm (solid), 5 mm (dotted), 10 mm (dash–dot), 20 mm (dash).

FCT method there is an increase in these attenuation maxima, and even a shift in the frequencies associated with them and the pass-band troughs. This could impose a rather severe frequency limit for engine simulations performed with those two schemes, which could only be overcome with a substantial increase in the computation time.

The results obtained with the Herschel-Quincke tubes confirm the previous comments. As an example, in Fig. 7 the influence of the mesh spacing on the transmission loss for the Lax–Wendroff and the FCT schemes is shown for geometry H-Q 4 (see Table 1 for the dimensions). Again, results from the Lax–Wendroff method are almost independent on mesh spacing, whereas the FCT method yields both a decrease in attenuation and a shift to higher frequencies as the mesh spacing is increased.

Up to this point, no reference has been made to the quality of the results obtained in terms of the ability of the methods to reproduce the expected behaviour of the configurations considered. In order to confirm this last point, in Fig. 8 the transmission loss for all the configurations, computed with a mesh spacing of 2 mm, is shown in the case of the Lax–Wendroff scheme (as seen before, for this mesh spacing results would be the same irrespective of the scheme chosen). In the case of the expansion chambers shown in Fig. 8(a), it is apparent that passbands are located, as expected, at frequencies given by the well-known expression $f/a = n/(2L)$ with n an integer and L the chamber length. The maximum values are also consistent with the expected behaviour. The situation is the same for the Herschel-Quincke ducts shown in Fig. 8(b), where in all the cases

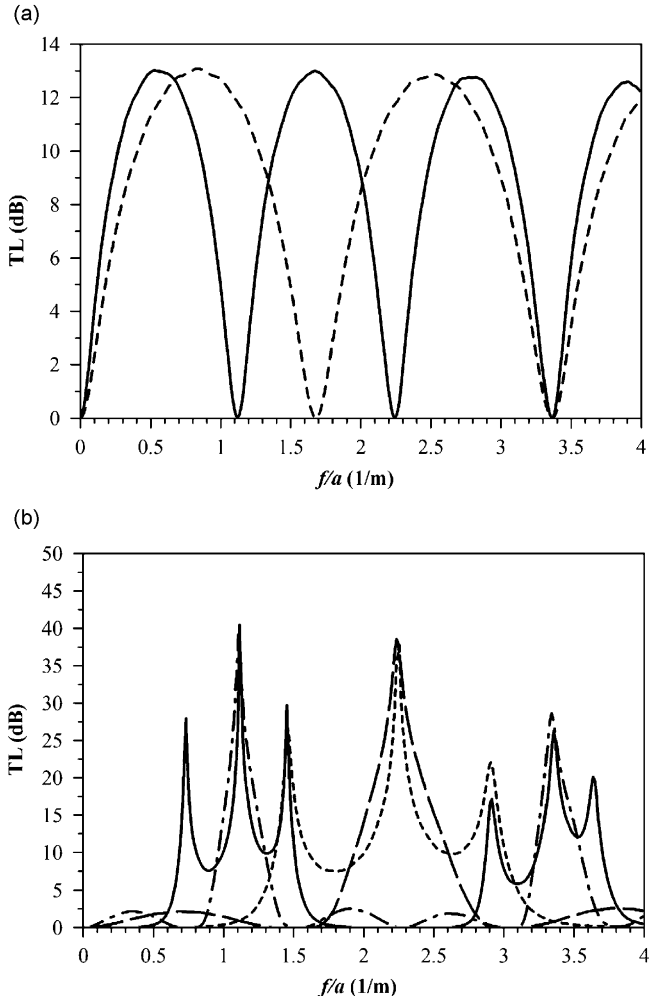

Fig. 8. Comparison of transmission loss computed with the Lax–Wendroff scheme and a mesh spacing of 2 mm: (a) expansion chambers: chamber 1 (solid), chamber 2 (dotted); (b) Herschel-Quincke tubes: H-Q 1 (solid), H-Q 2 (dotted), H-Q 3 (dash–dot), H-Q 4 (dash).

the attenuation spikes occur at frequencies given by $\sin kL_1/\sin kL_2 = S_1/S_2$, where k is the wavenumber and L_i and S_i are the length and cross section of the ith branch, respectively [19].

4. Conclusion

The performance of different numerical schemes, for the solution of the one-dimensional unsteady flow equations, when applied to the computation of the frequency response of exhaust mufflers has been tested and compared. In some cases, as the FCT scheme and the different implementations of the TVD concept, to the authors' knowledge such an evaluation had not been previously reported in the field of engine exhaust modelling.

Simple geometries with well-known acoustic behaviour, and sufficiently representative of attenuation mechanisms present in real mufflers, were chosen. A suitable methodology for the computation of the transmission loss was devised, and the necessary boundary conditions were defined and implemented. The study was focused on the quality of the results obtained, taking into account the sensitivity to the mesh spacing used and the computational cost. Also the theoretical computational cost required to achieve a certain accuracy has been analysed.

In this sense, it has been shown that good results may be obtained from any method if the mesh spacing is sufficiently small. However, when considering global engine simulations aiming at exhaust noise prediction, such small meshes may imply an excessive computation time. This represents a serious penalty for high-resolution schemes, which are considerably slower than simple centred schemes. In addition, these differences in computational time are higher if a certain accuracy is required since high-resolution schemes need more PPW.

The sensitivity of the different methods to the mesh spacing was then investigated, with the main conclusion that both the two-step Lax–Wendroff method and the CE–SE method do not exhibit an important influence of the mesh spacing, and thus relatively high values may be used without any loss of information. However, the fact that the Lax–Wendroff method (and, in general, simple schemes) is considerably faster suggests that it is a better option.

With respect to the other high-resolution schemes (FCT and TVD) they exhibit a considerable influence of the mesh spacing on the frequency results; therefore, they should not be considered as a valid option for exhaust noise prediction with global engine simulations, since the CE–SE method in comparably robust when sharp discontinuities are present in the flow and, being less sensitive to mesh spacing, provides a better compromise between the useful frequency range and the computation time required.

Acknowledgements

This work has been partially supported by MCYT through grant DPI2003-07153-C02-02.

Appendix A. Numerical schemes

The governing equations describing the one-dimensional non-homentropic gas flow, with the consideration of friction, heat transfer and area change, form a non-homogenous hyperbolic system [20]:

$$\frac{\partial \mathbf{W}}{\partial t}+\frac{\partial \mathbf{F}}{\partial x}+\mathbf{C}_1+\mathbf{C}_2=0. \tag{A.1}$$

This system, consisting of continuity, momentum and energy equations, is complemented by the equation of state or real gases properties [21]. In Eq. (A.1), $\mathbf{W}$ is the solution vector, $\mathbf{F}$ is the flux vector, $\mathbf{C}$ is the source term, making a distinction between the contribution of area (S) changes and that from friction and heat transfer, x is the spatial dimension and t is the time dimension. The one-dimensional gas flow governing equations are traditionally arranged in the vector form shown in Eq. (A.2):

$$\mathbf{W}=\begin{bmatrix}\rho\\ \rho u\\ \rho e_0\end{bmatrix},\quad \mathbf{F}=\begin{bmatrix}\rho u\\ p+\rho u^2\\ \rho u h_0\end{bmatrix},\quad \mathbf{C}_1=\begin{bmatrix}\rho u\\ \rho u^2\\ \rho u h_0\end{bmatrix}\frac{1}{S}\frac{\mathrm{d}S}{\mathrm{d}x},\quad \mathbf{C}_2=\begin{bmatrix}0\\ \rho G\\ -\rho q\end{bmatrix}, \tag{A.2}$$

where, assuming perfect-gas behaviour, the stagnation internal energy and the stagnation enthalpy may be written as $e_0=e+u^2/2=p/[(\gamma-1)\rho]+u^2/2$ and $h_0=h+u^2/2=\gamma p/[(\gamma-1)\rho]+u^2/2$, respectively, where c_v and c_p are the heat capacities at constant volume and constant pressure, respectively, γ is the ratio $\gamma=c_p/c_v$ and T is the absolute temperature. G is the friction term and q is the heat transfer term.

Recently, Gascón and Corberán [22] proposed a more conservative arrangement. This compact vector form includes the area in the solution vector and, as can be observed in Eqs. (A.3), the continuity equation and the energy equation are independent of the cross-section variation, and the momentum equation has a more compact form:

$$\mathbf{W}=\begin{bmatrix}\rho S\\ \rho u S\\ \rho e_0 S\end{bmatrix},\quad \mathbf{F}=\begin{bmatrix}\rho u S\\ S(p+\rho u^2)\\ \rho u h_0 S\end{bmatrix},\quad \mathbf{C}_1=\begin{bmatrix}0\\ -p\dfrac{\mathrm{d}S}{\mathrm{d}x}\\ 0\end{bmatrix},\quad \mathbf{C}_2=\begin{bmatrix}0\\ \rho G S\\ -\rho q S\end{bmatrix}. \tag{A.3}$$

In the following paragraphs, the different numerical methods are briefly described.

A.1. Lax–Wendroff method

The Lax–Wendroff method [23] is a centred second-order scheme in which the flow is approximated by the Taylor expansion. In order to avoid problems related with the evaluation of the Jacobian matrix, Richtmayer and Morton [24] proposed the so-called two-step Lax–Wendroff method, whose formulation for non-homentropic flow is as follows:

(i) First step:

$$w_{j+1/2}^{n+1/2} = (w_j^n + w_{j+1}^n)/2 - (f_{j+1}^n - f_j^n)\Delta t/(2\Delta x) - (c_j^n + c_{j+1}^n)\Delta t/4. \tag{A.4}$$

(ii) Second step:

$$w_j^{n+1} = w_j^n - (f_{j+1/2}^{n+1/2} - f_{j-1/2}^{n+1/2})\Delta t/\Delta x - (c_{j+1/2}^{n+1/2} + c_{j-1/2}^{n+1/2})\Delta t/2, \tag{A.5}$$

where subscripts refer to the mesh point and superscripts indicate the time step. Δt correspond to the time step and Δx to the mesh size.

A.2. MacCormack method

The version used here is that proposed in Ref. [9] and may be summarized as follows:

(i) First step (predictor):

$$\overline{w_j^{n+1}} = w_j^n - (f_{j+1}^n - f_j^n)\Delta t/\Delta x - (c_j^n + c_{j+1}^n)\Delta t/2. \tag{A.6}$$

(ii) Second step (corrector):

$$w_j^{n+1} = (\overline{w_j^{n+1}} + w_j^n)/2 - (\overline{f_j^{n+1}} - \overline{f_{j-1}^{n+1}})\Delta t/(2\Delta x) - (\overline{c_j^{n+1}} + \overline{c_{j-1}^{n+1}})\Delta t/4. \tag{A.7}$$

The bar over the superscript in Eq. (A.6) indicates that this is the first approximation taken in the predictor step, to be corrected in the second step. This notation is also used in Eq. (A.7) referred not only to the elements of the state vector **W**, but also to the elements of the flux vector **F** and the source vector **C**.

A.3. Flux corrected transport (FCT)

These techniques were developed by Boris and Book [25] in order to avoid non-physical overshoots produced by simple second-order schemes. As Niessner and Bulaty described later [26] these techniques consist of three different steps: transport, diffusion and anti-diffusion. The transport step obtains a preliminary solution at the next time step by means of a simple second-order scheme like Lax–Wendroff. Next, at the diffusion step, these results are post-processed applying an artificial smoothing operation to eliminate the gas property discontinuities. Finally, the anti-diffusion step recovers the second-order accuracy where diffusion is not needed to eliminate non-physical overshoots and the original solution is smooth.

Applying these techniques directly to vector **W** would lead, if source terms are present, to a violation in the conservation laws. For this reason, conservative parameters such as mass flow rate, stagnation enthalpy and stagnation pressure, given in Eqs. (A.8), should be used in the smoothing process instead of the components of vector **W** [27]:

$$\dot{m} = \rho u S, \quad h_0 = \frac{\gamma RT}{\gamma - 1} + \frac{u^2}{2}, \quad p_0 = p\left[1 + \frac{\gamma - 1}{2}\frac{u^2}{\gamma RT}\right]^{\gamma/(\gamma-1)}. \tag{A.8}$$

In this case, the non-physical overshoot can be eliminated and some of these techniques present TVD behaviour, and at the same time, the conservation laws are upheld.

A.4. TVD flux corrected scheme

Harten [28] applied a non-oscillatory first-order accuracy scheme to an appropriately modified flux function in order to obtain nonlinear schemes. These second-order schemes achieve a high-resolution while preserving the robustness of the original non-oscillatory first-order accuracy scheme. Originally, these techniques were conceived so as to obtain numerical approximation in weak solutions of the initial value problem for hyperbolic systems of conservation laws without source term. Later, Corberán adapted these techniques to non-homentropic flow based on formulation (A.3). This scheme can be written as

$$\mathbf{W}_j^{n+1} = \mathbf{W}_j^n - \frac{\Delta t}{\Delta x}[\hat{\mathbf{G}}_{j+1/2}^{\mathrm{TVD2}} - \hat{\mathbf{G}}_{j-1/2}^{\mathrm{TVD2}}] - \frac{\Delta t}{\Delta x}[\mathbf{B}_{j-1/2,j} + \mathbf{B}_{j,j+1/2}]. \tag{A.9}$$

Here, $\mathbf{B}$ is a vector representing the integral of the source term. Second-order accuracy is obtained by using the following flux:

$$\begin{aligned}\hat{\mathbf{G}}_{j+1/2}^{\mathrm{TVD2}} = \tfrac{1}{2}\{&\mathbf{F}_j + \mathbf{F}_{j+1} - \mathbf{B}_{j,j+1/2} + \mathbf{B}_{j+1/2,j+1} + \mathbf{P}_{j+1/2}(\mathbf{\Phi}_j + \mathbf{\Phi}_{j+1}) \\ &- \mathbf{P}_{j+1/2}h(\overline{\overline{\mathbf{D}}}_{j+1/2})[\mathbf{Q}_{j+1/2}(\mathbf{F}_{j+1} - \mathbf{F}_j + \mathbf{B}_{j,j+1}) + \mathbf{\Phi}_{j+1} - \mathbf{\Phi}_j]\}.\end{aligned} \tag{A.10}$$

Here, function h is chosen so that the entropy condition is preserved. In this case $\mathbf{\Phi}$ represents a second-order accuracy flux, which only acts when the solution is smooth.

A.5. TVD flux limiters

TVD flux limiter schemes, proposed by Sweby [29], consist of a first-order flux combined with a limited second-order flux. Davis [30] and Yee [31] also worked on these techniques approaching homentropic flow. In these flow conditions, the Davis flux limiter technique can be obtained just by adding a viscous term to the second step of the scheme proposed by Ritchmayer and Morton. This allows a substantial reduction in the computational time. The definition of the solution difference ratios used by this scheme to determine if a shock exists does not work using formulation (A.3); for this reason, Corberán adapted the Sweby flux limiter scheme to solve non-homentropic problems, using matrices what can increase computational time. The scheme can be written as

$$\mathbf{W}_j^{n+1} = \mathbf{W}_j^n - \frac{\Delta t}{\Delta x}[\hat{\mathbf{G}}_{j+1/2}^{\mathrm{SW}} - \hat{\mathbf{G}}_{j-1/2}^{\mathrm{SW}}] - \frac{\Delta t}{\Delta x}[\mathbf{B}_{j-1/2,j} + \mathbf{B}_{j,j+1/2}]. \tag{A.11}$$

Here the second-order accuracy flux can be calculated by means of the expression

$$\hat{\mathbf{G}}_{j+1/2}^{\mathrm{SW}} = \tfrac{1}{2}\{\mathbf{F}_j + \mathbf{F}_{j+1} - \mathbf{B}_{j,j+1/2} + \mathbf{B}_{j+1/2,j+1} - \mathbf{P}_{j+1/2}h(\overline{\mathbf{D}}_{j+1/2}^{\psi})\mathbf{Q}_{j+1/2}(\mathbf{F}_{j+1} - \mathbf{F}_j + \mathbf{B}_{j,j+1})_j\}, \tag{A.12}$$

where limiters are used to obtain the diagonal matrix $h(\vec{\mathbf{D}}_{j+1/2}^{\psi})$ and avoid overshoot. These limiters depend on the gradient relations, which allow shock detection. The gradient relations must also be re-defined in order to take into account the source term effects. The rest of the scheme is similar to the original one. This adaptation uses formulation (A.3).

A.6. Conservation element–solution element (CE–SE)

This scheme was proposed by Chang and To [32] for the homentropic problem and later adapted by Briz and Giannattasio [33] in order to allow consideration of source terms (formulation (A.2) was used). In this case, the numerical overshoot, typical of simple second-order schemes, is removed by replacing the simple averaging formula initially used with a weighted averaging formula. The space–time plane is divided into rhombic non-overlapping regions, referred to as solution elements (SE), centred at a mesh point, in which the solution is approximated by first-order Taylor series as

$$w_m(x,t;j,n) = (\sigma_m)_j^n + (\alpha_m)_j^n(x - x_j) + (\beta_m)_j^n(t - t_n), \quad m = 1,2,3. \tag{A.13}$$

Additionally, the space–time plane is also divided into rectangular regions that fill the space–time domain without overlap, called conservation elements (CE), in which the conservation laws are satisfied. In order to advance a half-time step the coefficients of all Taylor series of the next SE's must be calculated.

Appendix B. Management of boundary conditions

Previous work reported by Winterbone [34] indicates that the best solution is to try to use the same boundary conditions as for the method of characteristics by means of the generation, from the results of the finite-differences calculation, of auxiliary characteristic lines at the boundaries. This solution, as pointed out by Onorati [4,8], has the advantage that physical insight into the flow at the boundaries is preserved.

Considering that the positive direction of the flow is from left to right, it is always possible to find a λ line that passes through the right end of the duct at time $t+\Delta t$, whilst the value of β may be assumed to be, as a first approximation, the same as at time t. In the same way, a β line can always be found that passes through the left end of the duct if the flow is subsonic, and the corresponding λ value is assumed as in the previous case. When the flow is sonic or supersonic at the boundary, an artificial reduction to subsonic conditions is performed, making use of the Rankine–Hugoniot relations. The values assumed in each case as a first approximation are corrected by the equations of the boundary condition.

In the case of the path lines, distinction is required between outflow from the duct and inflow to the duct. If there is outflow at the right end of the duct then it is possible to define a path line that passes through the right end with a known value of the entropy level A_A, and similarly in the case of outflow at the left end. In case that there is inflow to the duct, the values obtained for the entropy level at the previous time step are assumed as a temporary solution.

All values, both known and guessed, are calculated by spatial interpolation from the u, a and p values computed for the previous time step. This interpolation should not be a simple linear interpolation between λ, β and A_A values since consistency problems could arise due to the eventual presence of temperature discontinuities [35], but between physical variables.

The interpolation procedure is similar to the bisection method. In Fig. B.1 the position diagram corresponding to the right end of the duct is represented (the case of the left end is analogous). The end has abscissa x_n and the neighbouring mesh point has abscissa x_{n-1}. The values of all the flow variables at time t are known, in particular for x_{n-1} and x_n, and the problem is to determine a λ line (or equivalently a path line: for our purposes, the only difference is the value of the slope) which passes through the end of the duct at time $t+\Delta t$. With the notation of Fig. B.1, this is equivalent to finding a point (y,t) with $y \in]x_{n-1}, x_n[$ such that the corresponding line contains the point $(x_n, t+\Delta t)$. This is afforded by constructing a sequence $\{y_k\}$ whose limit is point y. The first term of this sequence is taken to be the exact value for the homogeneous case, that is,

$$y_1 = x_{n-1} + \frac{x_n - x'_{n-1}}{x'_n - x'_{n-1}}(x_n - x_{n-1}) \tag{B.1}$$

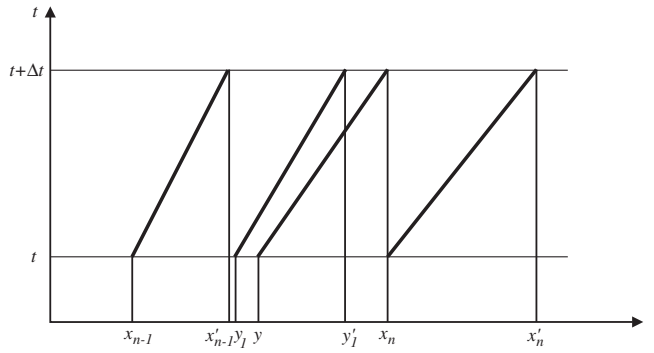

Fig. B.1. Connection with the boundary conditions: generation of a characteristic line at the end of a duct.

and the subsequent terms are defined as

$$y_k = y_{k-1} + \frac{x_n - x'_{n-1}}{x'_n - x'_{n-1}} \frac{x_n - y_{k-1}}{2}, \quad k > 1. \tag{B.2}$$

Finally, one takes $y = \lim_{k\to\infty} y_k$ but, in practice, this sequence converges very quickly and therefore it is only necessary to compute a few terms in order to achieve a suitable value for y.

When the corresponding line has been properly defined, the usual characteristic equations are used in order to determine the value of λ (or the entropy level A_A) at point $(x_n, t + \Delta t)$, taking into account friction losses, heat transmission and eventual area changes. At this point, the well-known boundary conditions for the method of characteristics may be used, and from the results obtained for the unknown Riemann variables at the end of the duct, the values of the physical variables and consequently those corresponding to the state variables considered here, are readily computed, allowing the calculation to proceed.

References

[1] F. Payri, A.J. Torregrosa, A. Broatch, D. Moya, Predictive modelling applied to exhaust system development, *Proceedings of the 2nd Styrian Noise, Vibration and Harshness Conference*, Graz, Austria, 22–23 May 2003.

[2] A.J. Torregrosa, A. Broatch, V. Bermúdez, I. Andrés, Experimental assessment of emission models used for IC engine exhaust noise prediction, *Experimental Thermal and Fluid Science* 30 (2) (2005) 97–107.

[3] A.D. Jones, Modelling the exhaust noise radiated from reciprocating internal combustion engines—a literature review, *Noise Control Engineering Journal* 23 (1) (1984) 12–31.

[4] A. Onorati, Prediction of the acoustical performances of muffling pipe systems by the method of characteristics, *Journal of Sound and Vibration* 171 (3) (1994) 369–395.

[5] A. Onorati, M. Perotti, S. Rebay, Modelling one-dimensional unsteady flows in ducts: symmetric finite difference schemes versus Galerkin discontinuous finite element methods, *International Journal of Mechanical Sciences* 39 (11) (1997) 1213–1236.

[6] F. Payri, J.V. Benajes, J. Galindo, J.R. Serrano, Modelling of turbocharged diesel engines in transient operation. Part 2: wave action models for calculating the operation in a high speed direct injection engine, *Proceedings of the Institution of Mechanical Engineers, Part D: Journal of Automobile Engineering* 216 (2002) 479–493.

[7] K.P. Mayer, B. Nowotny, Ein Berechnungsverfahren für Abgasschall-dämpfer von Viertaktmotoren, *MTZ Motortechnische Zeitschrift* 42 (10) (1981) 391–396.

[8] A. Onorati, Numerical simulation of exhaust flows and tailpipe noise of a small single-cylinder diesel engine, *SAE Paper 951755*, 1995.

[9] F. Payri, A.J. Torregrosa, M.D. Chust, Application of MacCormack schemes to IC engine exhaust noise prediction, *Journal of Sound and Vibration* 195 (5) (1996) 757–773.

[10] A. Onorati, Nonlinear fluid dynamic modeling of reactive silencers involving extended inlet/outlet and perforated ducts, *Noise Control Engineering Journal* 45 (1) (1997) 35–51.

[11] S. Takeyama, H. Takeda, Y. Takagi, Reduction in exhaust noise through valving modifications achieved with a gas dynamics simulation model, *SAE Paper 910617*, 1991.

[12] A. Selamet, N.S. Dickey, J.M. Novak, A time-domain computational simulation of acoustic silencers, *Journal of Vibration and Acoustics—Transactions of the ASME* 117 (3) (1995) 323–331.

[13] K.A. Kurbatskii, R.R. Mankbadi, Review of computational aeroacoustics algorithms, *International Journal of Computational Fluid Dynamics* 18 (6) (2004) 533–546.

[14] T. Colonius, S.K. Lele, Computational aeroacoustics: progress on nonlinear problems of sound generation, *Progress in Aerospace Sciences* 40 (2004) 345–416.

[15] N.S. Dickey, A. Selamet, Effects of numerical dissipation and dispersion on acoustic predictions from a time-domain finite difference technique for non-linear wave dynamics, *Journal of Sound and Vibration* 259 (1) (2003) 193–208.

[16] F. Payri, J. Galindo, J.R. Serrano, F.J. Arnau, Analysis of numerical methods to solve one-dimensional fluid-dynamic governing equations under impulsive flow in tapered ducts, *International Journal of Mechanical Sciences* 46 (7) (2004) 981–1004.

[17] F. Payri, J.M. Desantes, A. Broatch, Modified impulse method for the measurement of the frequency response of acoustic filters to weakly nonlinear transient excitations, *Journal of Acoustical Society of America* 107 (2) (2000) 731–738.

[18] F. Payri, J.M. Desantes, A.J. Torregrosa, Acoustic boundary condition for unsteady one-dimensional flow calculations, *Journal of Sound and Vibration* 188 (1) (1995) 85–110.

[19] A. Selamet, N.S. Dickey, J.M. Novak, The Herschel–Quincke tube: a theoretical, computational, and experimental investigation, *Journal of the Acoustical Society of America* 96 (5) (1994) 3177–3185.

[20] H. Daneshyar, *One-dimensional Compressible Flow*, Pergamon Press, Oxford, 1976.

[21] D.E. Winterbone, R.J. Pearson, A solution of the wave equations using real gases, *International Journal of Mechanical Sciences* 34 (12) (1992) 917–932.

[22] L. Gascón, J.M. Corberán, Construction of second-order TVD schemes for nonhomogeneous hyperbolic conservation laws, *Journal of Computational Physics* 172 (2001) 261–297.
[23] P.D. Lax, B. Wendroff, Systems of conservation laws, *Communications on Pure and Applied Mathematics* 17 (1964) 381–398.
[24] R.D. Richtmayer, K.W. Morton, *Difference Methods for Initial-value Problems*, Interscience, New York, 1967.
[25] J.P. Boris, D.L. Book, Flux-corrected transport I. SHASTA: a fluid transport algorithm that works, *Journal of Computational Physics* 11 (1973) 39–69.
[26] H. Niessner, T. Bulaty, A family of flux-correction methods to avoid overshoot occurring with solutions of unsteady flow problems, *Proceedings of the GAMM Conference of Numerical Methods of Fluid Mechanics*, Paris, France, 2003, pp. 241–250.
[27] J. Liu , N. Schorn, C. Schernus, L. Peng, Comparison studies on the method of characteristics and finite difference methods for one-dimensional gas flow through IC engine manifold, *SAE Paper 960078*, 1996.
[28] A. Harten, High resolution schemes for hyperbolic conservation laws, *Journal of Computational Physics* 49 (1983) 357–393.
[29] P.K. Sweby, High resolution schemes using flux limiters for hyperbolic conservation laws, *SIAM Journal of Numerical Analysis* 21 (1984) 995–1011.
[30] S.F. Davis, A simplified TVD finite difference scheme via artificial viscosity, *SIAM Journal of Scientific and Statistical Computing* 8 (1) (1987) 1–18.
[31] H.C. Yee, Construction of explicit and implicit symmetric TVD schemes and their applications, *Journal of Computational Physics* 68 (1987) 151–179.
[32] S.C. Chang, W.M. To, A new numerical framework for solving conservation laws—The method of space–time conservation element and solution element, *NASA TM 104495*, 1991.
[33] G. Briz, P. Giannattasio, Applicazione dello schema numerico conservation element—solution element al calcolo del flusso intazionario nei condotti dei motori a C.I, *Proceedings of the 48th ATI National Congress*, Taormina, Italy, 1993, pp. 233–247.
[34] D.E. Winterbone, R.J. Pearson, Z. Yong, Numerical simulation of intake and exhaust flows in a high-speed multi-cylinder petrol engine using the Lax–Wendroff method, *Proceedings of the Institution of Mechanical Engineers Computers in Engine Technology Conference*, Cambridge, UK, September 1991.
[35] F. Payri, F. Boada, J.M. Corberán, Modifications to the method of characteristics for the analysis of the gas exchange process in internal combustion engines, *Proceedings of the Institution of Mechanical Engineers, Part D: Journal of Automobile Engineering* 200 (4) (1986) 259–266.